International Journal of Earth, Energy and Environmental Sciences
ISSN: 2517-942X
Vol:9, No:5, 2015

Corrosion Monitoring of Weathering Steel in a Simulated Coastal-Industrial Environment

Ch. Thee, Junhua Dong, Wei Ke

Abstract**—**The atmospheres in many cities along the coastal lines in the world have been rapidly changed to coastal-industrial atmosphere. Hence, it is vital to investigate the corrosion behavior of steel exposed to this kind of environment. In this present study, Electrochemical Impedance Spectrography (EIS) and film thickness measurement were applied to monitor the corrosion behavior of weathering steel covered with a thin layer of the electrolyte in a wet-dry cyclic condition, simulating a coastal-industrial environment at 25^{o}C and 60% RH. The results indicate that in all cycles, the corrosion rate increases during the drying process due to an increase in anion concentration and an acceleration of oxygen diffusion enhanced by the effect of the thinning out of the electrolyte. During the wet-dry cyclic corrosion test, the long-term corrosion behavior of this steel depends on the periods of exposure. Corrosion process is first accelerated and then decelerated. The decelerating corrosion process is contributed to the formation of the protective rust, favored by the wet-dry cycle and the acid regeneration process during the rusting process.

Keywords**—**Atmospheric corrosion, EIS, low alloy, rust.

I. Introduction

THE atmospheres in many cities along the coastal lines in the world have been rapidly changed to coastal – industrial atmosphere. In this kind of environment, the combined effect of Chlorides and sulphur dioxide (SO_2) is complicated and much far from clear [1]-[3]. Hence, it is of great interest to perform the corrosion monitoring technique to investigate the corrosion behavior of steel, particularly in the long-term exposure.

In the past, many investigations on the atmospheric corrosion of steel were conducted based on the long-term filed exposure test [1]-[3]. This method can provide very important information about the long-term durability of steel exposed to the real environments in terms of the estimated corrosion rate and the rust morphology [3]-[5]. These results are very useful, but it takes a long time just for one evolution assessment [6], [7].

To compensate this disadvantage, simulated atmospheric corrosion tests for the acceleration of corrosion have been developed since last decade [7], [8]. Wet/dry cyclic corrosion test based on saltwater spray followed by drying can accelerate and simulate atmospheric corrosion under controlled humidity and temperature. Nowadays, Electrochemical Impedance Spectrography (EIS) is proven to be an effective method to study the atmospheric corrosion behavior of low alloy steels [9], [10]. So, there are many researches using this technique to observe the corrosion behavior of steel [11]-[13]. However, there have been few studies trying to elucidate the atmospheric corrosion behavior of weathering steel under the combined effect of Chlorides and sulphur dioxide.

In this present work, EIS and thickness measurements were employed to study the corrosion behavior of weathering steel under a thin electrolyte film submitted to alternate wet-dry conditions in a simulated coastal-industrial environment maintained at 25°C and 60% RH (relative humidity). This research was started primarily to investigate the electrochemical corrosion behavior of this steel during the evaporation of the electrolyte. Special attentions were paid to the evolution of the charge transfer resistance and the rust resistance during long-term exposure. Furthermore, the corrosion evolution mechanism based on the analyzed results was also discussed.

II. Experimental Procedures

A. Electrode Preparation

In this study, weathering steel was used as the electrode material and its composition was (in mass %): 0.06 C, 0.0135 Si, 1.16 Mn, 0.38 Cr, 0.16 Ni, 0.24 Cu, 0.019 P, 0.005 Si, and Fe. The steel was sectioned into a pair of comb-like electrodes. Then, the two electrodes were embedded in epoxy resin with the comb fingers crossing ,but not contacting each other as schematically shown in Fig. 1, and the surface area of the two-electrode was approximated 1 cm2. After being ground on SiC paper to 1000 grits, the two-electrode cell was stored in a desiccator for 24 h and then subjected to the wet-dry cyclic corrosion tests.

B. Simulation Conditions and Wet-Dry Cyclic Corrosion Tests (CCT)

The simulated environmental condition in this experimental chamber was maintained at 25°C with a constant RH of 60% by using the humidity control system containing water-glycerol mixture, the ratio of which was prepared according to ASTM D 5032 [14].

The CCT was performed as follows. The first CCT was conducted by wetting the electrode surface with 0.05 mol L^{-1} NaCl solution (simulating a coastal environment) with an approximate volume of 50 μL cm^{-2}, and drying it for 12 h. For other CCT cycles, the same working steps as the first CCT were repeated, but a same volume of distilled water was used as a

Ch.Thee is with The material engineering program , Faculty of Engineering , Burapha University, Chonburi 20131, Thailand (phone: +86 24 2391 5912; fax: +86 24 2389 4149 ; e-mail: thee@eng.buu.ac.th).

Junhua Dong is with State Key Laboratory for Corrosion and Protection, Institute of Metal Research, Chinese Academy of Sciences, Wencui Road 62, Shenyang 110016, China (e-mail: jhdong@imr.ac.cn).

Wei Ke is with State Key Laboratory for Corrosion and Protection, Institute of Metal Research, Chinese Academy of Sciences, Wencui Road 62, Shenyang 110016, China (e-mail: kewei@imr.ac.cn).

solution to keep a constant amount of chloride ions during the whole test. The whole experiment for all exposure conditions was performed for at least 60 CCT numbers.

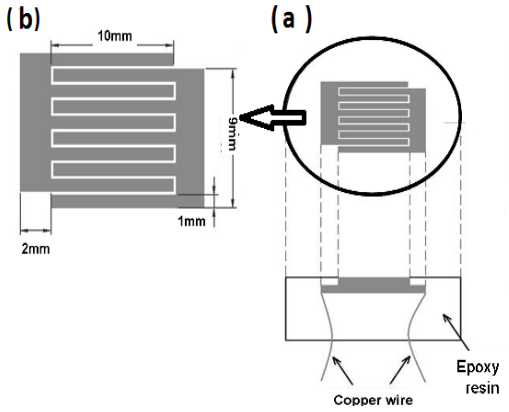

Fig. 1 Schematic diagram of the electrode cell used (a) electrode cell with two views and (b) the enlarged top view

C. Electrolyte Thickness and EIS Measurements

During the whole test, the electrode cell has been placed on an analytic balance BS 224 S, Satorius with accuracy d = 0.1 mg, and its USB interface is connected with a computer for recording the data of the weight change. When the electrolyte is laid on the surface of the cell, the observed weight of the electrolyte is read and then recorded in the computer.

The weight of the electrolyte film (*We*) can be gained as:

$$We = Ws - Wd \quad (1)$$

where Ws stands for the observed weight of the cell during the evaporation process; Wd is the initial weight of the cell for the first CCT, and is the weight of the dried rusted-cell when a new CCT cycle starts. The thickness of electrolyte film (X) can be monitored by (2):

$$X = \frac{W_e}{\rho S} \quad (2)$$

where ρ and S are the density and surface area of the electrolyte film. In this study, ρ is 1000 mg cm^{-3} and S is considered to be 1 cm^2.

Cyclic EIS measurements were continuously carried out during the evaporation of the electrolyte until the surface is completely dried. The frequency range for EIS was from 100 kHz to 10 mHz with the amplitude of 5mV (RMS) using a.c signals at open circuit potential.

III. Results

A. Thickness and EIS Measurements on Steel Substrate Electrode Cell

Fig. 2 showed the changes of the electrolyte film thickness and the concentration of Cl^- and SO_4^{2-} during the electrolyte evaporation process on the steel substrate sample in the first CCT. The numbers 1-15 in the plot denote the sequence of the cyclic EIS measurements with the calculated electrolyte film thickness results. Obviously, the electrolyte film thickness shows a linear decrease until zero with its evaporation. When the corrosion proceeds to 2.03 h, the weight becomes zero, indicating the complete thinning out of the electrolyte film, and the thickness of which is denoted by 0 μm. In addition, Fig. 1 also shows the changes in concentration of chloride ion and sulphate ion during the thin electrolyte film evaporation process. Apparently, the concentration of Cl^- and SO_4^{2-} increases with a low rate and then significantly increases with the electrolyte layer thinning out. When the electrolyte layer is approaching thinning out, the concentration of Cl^- and SO_4^{2-} rises to saturation or oversaturation, recrystallizing to very fine particles of NaCl and Na_2SO_4, precipitated on the steel substrate surface.

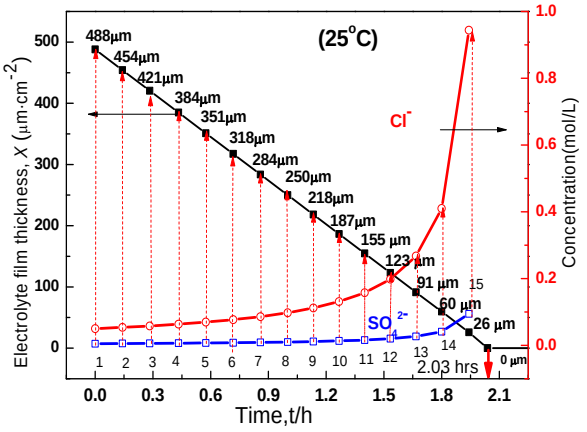

Fig. 2 Variation in weight and thickness of the electrolyte film during its evaporation process on un-rusted steel sample in the first CCT

Fig. 3 (a) reveals that, as the evaporation process of the electrolyte film proceeds, the impedance at both high frequency and low frequency firstly tends to decrease until the 13th EIS measurement, and then sharply increases for the 14th EIS measurement. For the steel substrate, the iron dissolution is balanced with the oxygen reduction [24], and during the period of 1st -15th EIS measurements, the oxygen reduction rate (1) increases due to the ready availability of dissolved oxygen from the air to the thinning electrolyte film, leading to the increased corrosion rate and variation in high frequency impedance and low frequency impedance as the EIS measurement proceeds.

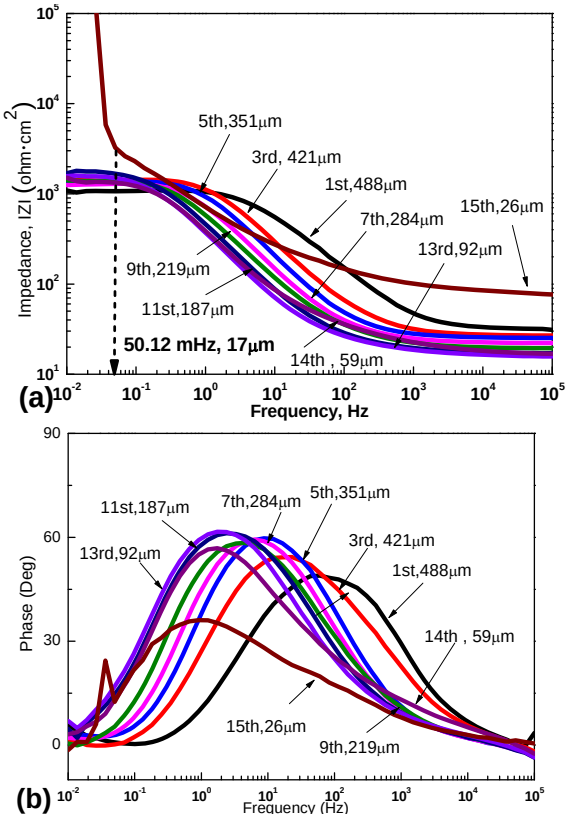

Fig. 3 The Bode results for EIS measurement on fresh steel sample in the first CCT. (a) Impedance plot (b) Phase angle plot

Besides, the increase in a concentration of Cl^- and SO_4^{2-} in the thinning electrolyte film attributed to an enhanced electrical conductivity of the electrolyte, accelerating the steel corrosion process [12], [15], [16]. Therefore, the increased concentration of Cl^- and SO_4^{2-} in the thinning electrolyte film may also be responsible for the decreased high frequency impedance and low frequency impedance during the period of 2nd -14th EIS measurements. For the 15th EIS measurement carried out with an electrolyte film thickness of 26 μm, the impedance at the high frequency significantly increases and subsequently shows an abrupt increase at frequency of 50.12 mHz, at which point the electrolyte thickness is about 17 μm. This impedance change can be explained as follow: when the remaining electrolyte film thickness is thinner than 17 μm, the electrolyte cannot be continuously distributed on the steel surface. In addition, the corrosion rate has reached a maximum value when the layer thickness is thinner than 26 μm.

Fig. 3 (b) shows that for the 1st -15th phase angle curves, the phase angle peak exhibits a shift to the direction of lower frequency side as the electrolyte evaporation proceeds due to the existence of Cl^- and SO_4^{2-} in the electrolyte layer [29]. Besides, a great decrease in the peak especially at the lower frequency side of the phase angle curves of 15th EIS measurement is apparently observed, meaning a significant change in the steel surface condition [17].

B. Thickness and EIS Measurements on Steel Substrate Electrode Cell

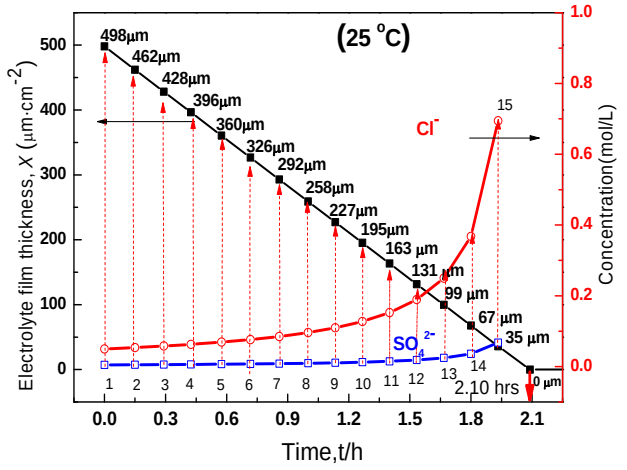

Fig. 4 Variation in weight and thickness of the electrolyte film during its evaporation process on rusted steel sample in the first CCT

Fig. 4 shows the changes in the electrolyte film thickness and the concentration of Cl^- and SO_4^{2-} during the electrolyte evaporation process on rusted steel sample in the 58th CCT. The numbers 1-15 in Fig. 4 denote the sequence of the cyclic EIS measurements, and the corresponding electrolyte film thickness result has also been given. Similar to the results shown in Fig. 2, the electrolyte thickness gradually becomes thinner and thinner until zero as the electrolyte film evaporation proceeds. Fig. 4 also indicates that for the rusted steel sample during the 58th CCT, the initial thickness of 498 μm electrolyte film electrolyte film does not drop to zero until the corrosion proceeds to 2.10 h. However, Fig. 2 indicates that for the steel substrate sample, it takes 2.03 h to evaporate out the initial thickness of 488 μm electrolyte. Principally, the amount of water covering the surface is a function of temperature, porosity, degree of oxidation, grain structure, and a variety of other surface-related properties [1]-[3]. Therefore, the prolonged time of wetness on the rusted steel surface is caused by the formation of rust layer [12], [13]. In addition, Fig. 4 shows the change in the concentration of Cl^- and SO_4^{2-} during evaporation process of the thin electrolyte film. Obviously, the concentration of Cl^- and SO_4^{2-} firstly exhibits a gradual increase and then followed by a significant increase with the electrolyte layer thinning out. When the electrolyte layer approaches 0 μm, the concentration of Cl^- and SO_4^{2-} rises to saturation or oversaturation, recrystallizing to very fine particles of NaCl and Na_2SO_4, precipitated on the steel substrate surface.

Fig. 5 shows the Bode plots of the EIS results obtained on the rusted steel sample during the 58th wet-dry cyclic corrosion test, and the sequence of the cyclic EIS measurements is displayed by 1st -15th.

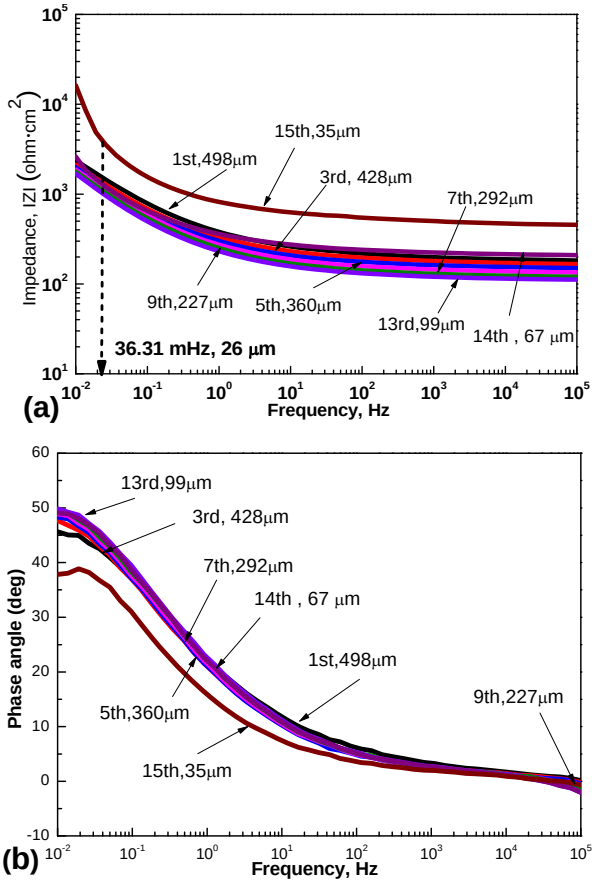

Fig. 5 The Bode results for EIS measurement on rusted steel sample in the first CCT. (a) Impedance plot; (b) Phase angle plot

Generally, for the impedance of the Bode plot measured on the rusted steel substrate, the rust layer resistance is dominated at high frequency and the sum of rust layer resistance and charge transfer resistance at the rust/steel interface is dominated at low frequency [18], [19]. The fact that the phase angle in Fig. 5 (b) at high frequency is close to 0^{o} also indicates the high frequency-dominated rust layer resistance [19], which also refers to the solution resistance in penetrating the rust layer to steel substrate [20]. Fig. 5 (a) shows that the impedance at both high frequency and low frequency decreases as the evaporation process proceeds during the 1st-14th EIS measurements, indicating an accelerating corrosion behavior of the steel sample during the period of time. Nevertheless, for the 15^{th} EIS measurement carried out with an electrolyte film thickness of 35 μm, the impedance at the high frequency obviously increases and then shows an abrupt increase at frequency of 36.31 mHz, at which point the electrolyte thickness is about 26 μm. This impedance change indicates that, when the remaining electrolyte film thickness is less than 26 μm, the electrolyte cannot be continuously distributed on the rusted steel surface and the corrosion rate of the steel sample sharply decreases. Besides, the corrosion rate has reached a maximum value when the layer thickness is thinner than 35 μm.

IV. Discussion

In order to investigate the corrosion evolution of this weathering steel under a thin electrolyte film during the wet-dry cyclic corrosion tests, we continuously monitored the impedance evolution in the high frequency, 10 kHz, and low frequency, 10 mHz. The polarization impedance (Rp) can be obtained by subtracting the high frequency impedance from the low frequency impedance and this impedance is considered an indication of the corrosion rate. For the high frequencies impedance, it is regarded as the resistance of the rust (R_{rust}), which indicates the resistance of the electrolyte in the fine pores in the rust layer [19]-[23].

A. Evolution in Resistance of the Rust Layer

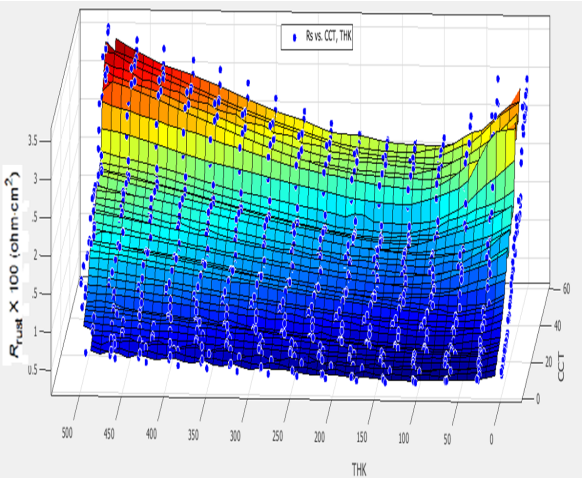

Fig. 6 The evolution of the rust resistance during the CCT

Fig. 6 shows the evolution in R_{rust} as a function of CCT number for each EIS measurement during the initial and the subsequent wet-dry cyclic process, respectively. It can be found that during each wet-dry cycle, Rr_{ust} gradually decreases with the evaporation of the electrolyte and then abruptly increases. As the electrolyte evaporates, R_{rust} decreases due to an increase in the concentration of Cl^{-} and SO_4^{2-} in the electrolyte as indicated in Figs. 2 and 4 [12], [15], [16], which results in the penetration of more anions through the rust layer and the increased conductivity of the electrolyte in the fine pores in the rust layer. These findings mean a decrease in R_{rust}. However, before the electrolyte drying out, R_{rust} abruptly increases. When the electrolyte is extremely thin or, the liquid film would not be continuous and thus the corrosion cell is just the electrodes [24]-[28]. In addition, the results from Fig. 6 also represent the evolution in the rust layer resistance R_{rust} is a function of CCT number. From this figure, R_{rust} increases with an increase in the numbers of CCT and during the initial stage the rust layer resistance R_{rust} is quite low. Nevertheless, during the subsequent stage of CCT, R_{rust} increase greatly with an increase in the CCT number. The remarkable corrosion resistance of a metal is usually attributed to the formation of a compact and adhesive rust layer on its substrate [11], [12]. During the initial stage of corrosion, the rust layer is very loose, porous and discontinuous. It is therefore non-protective [17]. As the

corrosion process proceeds to the subsequent stage, the rust layer becomes more compact and adhesive to the steel substrate [28], [29] and thereby the barrier effect of the rust layer is improved. Hence, the significant increase in rust resistance in the subsequent period of CCT can be ascribed to the improved barrier effect of the rust layer [30], [31].

B. Evolution in the Charge Transfer Resistance

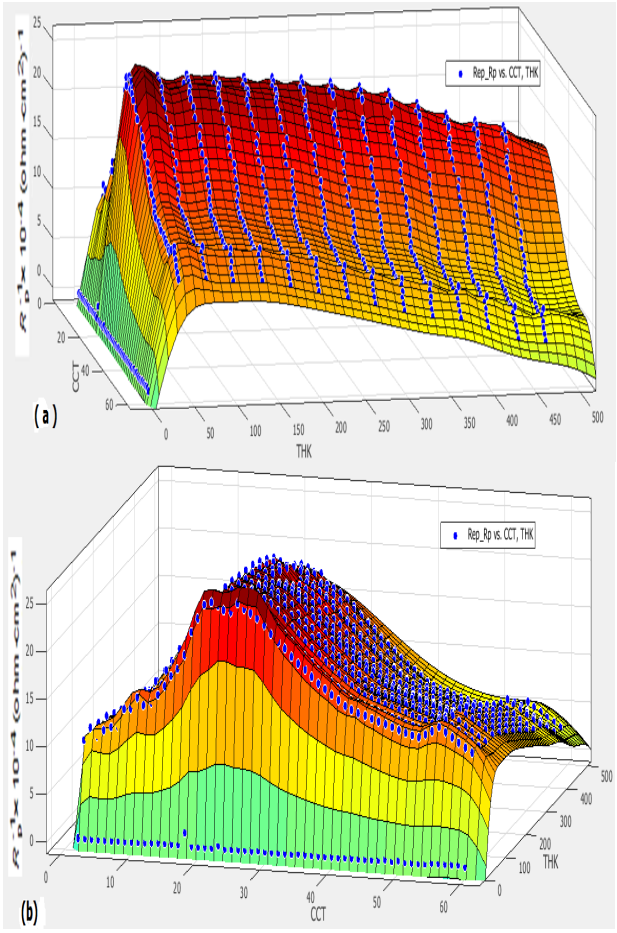

Fig. 7 The evolution of Rp^{-1} during the CCT process (a) the coordinate of Rp^{-1} (Ohm cm^2)$^{-1}$ and the electrolyte thickness (THK: μm), and b) the coordinate of Rp^{-1} and CCT (cycle)

The evolution of Rp^{-1} as a function of electrolyte thickness and CCT number for whole CCT is demonstrated in Fig. 7. Fig. 7 (a) showed that in the coordinate of Rp^{-1} and the electrolyte thickness for four controlled temperatures, Rp^{-1} tends to gradually increase with a decrease in the electrolyte thickness. Rp^{-1} reaches the maximum value before the surface of steel completely dries. The reduction of the electrolyte thickness accelerates the corrosion of this steel by enhancing the transport of O_2 and increasing concentration [9]-[12]. With the rust covered–substrate, rust reduction also accelerates corrosion, leading to a further accelerating corrosion process.

Fig. 7 (b) indicated that in Rp^{-1} -CCT number relationship for this steel of all cases, corrosion process accelerates in the initial stage and decelerates in the later stage. In the first stage, the rust is thin, porous and discontinuous, which cannot afford the effective barrier effect to resist the transport of corrosion agents like chloride and sulphate ions. In addition, the rust in this stage usually contains large portions of reducible FeOOH. The electrochemical transformation of this phase also causes an acceleration of the cathodic reaction. Hence, the corrosion accelerates in the first stage. Nevertheless, with the prolonged CCT, the rust grows in the size and thickness and then becomes more compact and thicker. This rust can effectively resist the diffusion of those anions. Furthermore, in case of the thick rust-covered steel substrate, amount of unstable rust constituents in the grown rust becomes less abundant, which further protects the substrate. Thus, the corrosion process in the later stage decelerates.

C. Corrosion Mechanisms

Atmospheric corrosion of weathering steel proceeds under the thin layers of electrolyte and in practice, steel has to be subjected to several wet-dry cycles, which causes the formation of the rust [11]-[14]. For the steel with no rust, the oxygen reduction or hydrogen evolution and metal dissolution dominate the corrosion process [15]-[17]. Next, during the first CCT, the dissolved ferrous ions are hydrolyzed into Ferrous Hydroxide. Then, during the drying process of electrolyte, Ferrous Hydroxide can be oxidized into Ferrous ions or Ferric ions [30], [31]. These ions are electrochemically active and can subsequently be transformed into a large amount of FeOOH [30], [31]. Furthermore, due to the availability of Cl^-, SO_4^{2-} in the electrolyte, the formation of Iron Chloride, and Iron Sulphate can also take place [1], [31]. Accordingly, at least three components of corrosion products possibly precipitate on the substrate and provide the retarding effect on the corrosion process in the beginning of the evaporation process. However, when the layer of electrolyte turns thinner, the effect of increasing in the transport of oxygen and anions toward the substrate layer caused by a decrease in the electrolyte layer is predominant over the inhibiting effect of the corrosion process by the initial rust [6]. Hence, the corrosion rate increases as the electrolyte thickness becomes much thinner.

For subsequent wet-dry cycles of weathering steel during the initial corrosion stage, the corrosion products gradually grow to cover the whole surface of the electrode. This results in lowering the active area of oxygen reduction or hydrogen reduction. Moreover, the Ferric Oxyhydroxide, one of corrosion product, is not stable and tends to be transformed to magnetite during the drying process [32]. At the same time, with the presence of water and oxygen, Iron sulphate and Iron Chloride can also be hydrolysed to produce Ferric Oxy hydroxide [31], [32]. In case of the Hydrolysed Iron Sulphate, sulphuric acid is also re-generated and continues to react with the freshly dissolved Fe ions to generate new ferrous sulphate in accordance with the acid regeneration cycle theory [33], [34]. As discussed previously from Fig. 7, the corrosion evolution is found to depend on the durations of CCT. During the initial stage, when more and more areas of electrode are covered with rust, the role of oxygen reduction or hydrogen reduction in the corrosion process becomes more and more

restricted. Conversely, the role of the rust reduction enhanced by the regeneration of sulphuric acid turns more primary [34]-[37], which results in an increase in the corrosion rate in the initial corrosion stage. At around 25 CCT, where corrosion rate reach maximum, the advantage of the protectiveness of the growing rust layers becomes in balance with the negative effect of the corrosion. After this CCT, with the higher amount of accumulated rust layer on the substrate, the corrosion rate tends to decrease [38]-[40]. In addition, as exhibited from Fig. 6, the rust can play an important role on the corrosion process. In the initial stage, the maximum corrosion rate increases significantly. This indicates the unstable rust, which cannot provide the effective barrier effect to resist the corrosion process. After 25CCT, the rust layers still continue growing. The decrease in the corrosion rate in Fig. 7 indicates the enhanced protectiveness of the rust layers in this stage. Therefore, our results point out that the decreased corrosion rate in the subsequence stages is due to the formation of the stable rust, which is formed due to the combined effect of increasing wet-dry cycles and acid regeneration cycle. With the developing process of the rust during CCT, the corrosion resistant properties of this steel gradually increases. As a result, the corrosion rate of weathering steel exposed to the simulated coastal – industrial environment become lower in the second stage.

IV. Conclusion

The corrosion monitoring of weathering steel covered with thin electrolyte layers was carried out under alternate wet-dry cyclic conditions simulating a coastal – industrial environment at 25°C and 60 %RH. The following conclusions were drawn:

1. In general, corrosion rate of each CCT increases during the drying process of the electrolyte due to an increase in the concentration of chloride and sulphate ions as well as an enhancement of oxygen diffusion caused by the effect of the evaporation process of the electrolyte.
2. The corrosion kinetics depends on the durations of exposure and can be divided into two stages. The corrosion is accelerated in the initial stage. Around 25th CCT, the useful effect of rust is in balance with the adverse effect of the corrosion process, the corrosion rate reaches the maximum value. Then, the corrosion rate significantly decreases.
3. The enhanced protectiveness of the rust layer in the second stage of CCT of weathering steel in a simulated coastal – industrial environment is found to be related to the presence of the more stable rust. The wet – dry cycle and acid regeneration cycle favored the formation of the stable rust by accelerating the dissolution and precipitation in the rusting process.

Acknowledgment

The authors would like to express sincere thanks to the National Science Fund of China under the Contract Nos. 51201170, 51131007, 50499336 and 50971120, and to Royal Thai Government Scholarship for financial support for Ch. Thee. The Authors also wish to thank Dr. Yossiri Ariyakul for his contribution in data analysis.

References

[1] J. H. Dong, E. H. Han, W. Ke, "Introduction to atmospheric corrosion research in China", Sci. Technol. Adv. Mater., vol.8, 2007, pp. 559–565.
[2] W. J. Chen, Long Hao, Junhua Dong, Wei Ke, "Effect of sulphur dioxide on the corrosion of a low alloy steel in simulated coastal industrial atmosphere", Corros. Sci., vol.83 ,2014, pp.155–163
[3] C. Leygraf, T. Graedel, Atmospheric Corrosion, John Wiley & Sons, Inc., New York, 2000.
[4] M. Stratman, H. Streckel, "On the Atmospheric Corrosion of Metal which are covered with thin electrolyte layers–II. Experimental Results". Corros. Sci., vol. 30, 1990, pp. 697–714.
[5] M. Stratman, H. Streckel, "On the Atmospheric Corrosion of Metal which are covered with thin electrolyte layers–III. The measurement of polarisation curves on metal surfaces which are covered by thin electrolyte layers". Corros. Sci., vol. 30,(1990, pp. 715–734.
[6] N. D. Tomashov, Development of the electrochemical theory of metallic corrosion, Corrosion, vol. 20, 1964, pp. 7–14.
[7] L. Hao, S. X. Zhang, J. H. Dong, W. Ke, "Rusting evolution of MnCuP weathering steel submitted to simulated industrial atmospheric corrosion, Metall. Mater. Trans. A, vol. 43, 2012, pp. 1724–1730.
[8] J. Dong, J. H. Dong, E. H. Han, "Rusting evolvement of mild steel under wet/dry cyclic condition with pH 4 NaHSO3 solution", Corros. Sci. Prot. Technol., vol. 21, 2009, pp. 1–4.
[9] T. Tsuru, A. Nishikata, J. Wang, "Electrochemical studies on corrosion under a water film", Mater. Sci. Eng. A, vol.198, 1995, pp.161–168.
[10] A. Nishikata, Y. Ichihara, Y. Hayashi, T. Tsuru, "Influence of electrolyte layer thickness and pH on the initial stage of the atmospheric corrosion of iron", J. Electrochem. Soc., vol. 144, 1997, pp. 1244–1252.
[11] L. Hao, S. X. Zhang, J. H. Dong, W. Ke, "Evolution of atmospheric corrosion of MnCuP weathering steel in a simulated coastal-industrial atmosphere", Corros. Sci., vol. 59, 2012, pp. 270–276.
[12] Ch. Thee, L. Hao, J. H. Dong, X. Wie, X. F. Li, W. Ke, "Atmospheric corrosion monitoring of a weathering under an electrolyte film in cyclic wet-dry condition", Corros. Sci., vol. 59, 2012, pp. 270–276.
[13] L. Hao, S. X. Zhang, J. H. Dong, W. Ke, "Atmospheric corrosion resistance of MnCuP weathering steel in simulated environments", Corros. Sci., vol. 53, 2011, pp. 4187−4192.
[14] ASTM D 5032-97 , Standard Practice for Maintaining Constant Relative Humidity by Means of Aqueous Glycerin Solutions, ASTM International, West Conshohocken, PA, 2003.
[15] X. X. Fu, J. H. Dong, E. H. Han, W. Ke, "A new experimental method for in situ corrosion monitoring under alternate wet- dry conditions", Sensors, vol.9, 2009, pp. 10400–10410.
[16] S. X. Li, J. H. Dong, E. H. Han, W. Ke, "Evolvement of electrochemical impedance spectra of a bi-electrode cell for carbon steel in the initial stage of wet/dry process", Corros. Sci. Prot. Technol., vol.19, 2007, pp. 167–170.
[17] L. Hao, S. X. Zhang, J. H. Dong, W. Ke, "Corrosion evolution of MnCuP weathering steel submitted to wet/dry cyclic tests in a simulated coastal atmosphere", Corros. Sci., vol. 58, 2012, pp. 175–180.
[18] I. M. Allam, J. S. Arlow, H.Saricimen, "Initial stage of atmospheric corrosion of steel in The Arabian gulf", Corros. Sci., vol. 32, 1991, pp. 417–432
[19] W. J. Lorenz, F. Mansfeld, "Determination of corrosion rates by electrochemical DC and AC methods", Corros. Sci., vol. 21, 1981, pp. 647–672.
[20] F. Masfeld, S. Lin, Y. C. Chen, "Minimization of high-frequency phase-shifts in impedance measurements", J. Electrochem. Soc., vol. 135, 1988, pp. 906–907.
[21] R. G. Kelly, J. R. Scully, D. W. Shoesmith, R. G. Buchheit, Electrochemical techniques in corrosion science and engineering, Marcel Dekker Inc, 2002. R. Evans, "Mechanism of atmospheric rusting", Corros. Sci., vol. 9, 1969, pp. 813–821.
[22] M. E. Orazem, B. Tribolet, Electrochemical Impedance Spectrography, John Wiley & Sons, Inc., New Jersey, 2008.
[23] C. N. Cao, Principles of Electrochemistry of Corrosion, Chemical Industry Press, Beijing, 2004.
[24] S. H. Zhang, S. B. Lyon, "Anodic processes on iron covered by thin, dilute electrolyte layers (I)–Anodic Polarisation", Corros. Sci., vol.36, 1994, pp.1289–1307.

[25] S. H. Zhang, S. B. Lyon, "Anodic processes on iron covered by thin, dilute electrolyte layers (II)–AC impedance measurements", Corros. Sci., vol 36, 1994, pp. 1309–1321.
[26] A. P. Yadav, A. Nishikata, T. Tsuru, "Electrochemical impedance study on galvanized steel corrosion under cyclic wet-dry conditions–influence of time of wetness", Corros. Sci., vol. 46, 2004, pp. 169–181.
[27] A. P. Yadav, A. Nishikata, T. Tsuru, "Evaluation of impedance spectra of zinc and galvanised steel corroding under atmospheric environments", Corros. Eng. Sci. Technolo., vol .45, 2008, pp. 23–29.
[28] A. Nishikata, F. Suzuki, T. Tsuru, "Corrosion monitoring of nickel-containing steels in marine atmospheric environment", Corros. Sci., vol. 47, 2005, pp. 2578–2588.
[29] Ch. Thee, Long Hao, Junhua Dong, Mu Xin, Wei Ke, "One numerical approach for atmospheric corrosion monitoring based on EIS of a weathering steel ", Acta Metallurgica Sinica (English Letter), 2014. DOI 10.1007/s40195-014-0193-5.
[30] T. Nishimura, H. Katayama, K. Noda, T. Kodama, "Electrochemical behavior of rust formed on carbon steel in a wet/dry environment containing chloride ions", Corrosion, vol. 56, 2000, pp. 935–941.
[31] D.D.N. Singh, S. Yadav, J.K. Saha, "Role of climate conditions on corrosion charecteristics of structural steels", Corros. Sci., vol. 50, 2008, pp.93–110.
[32] U. R. Evans, "Mechanism of atmospheric rusting", Corros. Sci., vol. 9, 1969, pp. 813–821
[33] T. Misawa, T. Kyuno, W. Suëtaka, S. Shimodaira, "The mechanism of atmospheric rusting and the effect of Cu and P on the rust formation of low alloy steel", Corros. Sci., vol. 11, 1971, pp. 33–48.
[34] T. Misawa, "The mechanism of atmospheric rusting and the protective amorphous rust on low alloy steel", Corros. Sci., vol. 14, 1974, pp. 279–289.
[35] J. H. Wang, F. I. Wei, Y. S. Chang, H. C. Shih, "The corrosion mechanisms of carbon steel and weathering steel in SO2 polluted atmospheric", Mat. Chem. Phys., vol.47, 1977, pp. 1-8.
[36] E. Mccafferty, Introduction to Corrosion Science, Springer science and Business Media, New York, 2010.
[37] K. Bartoň, Protection against atmospheric corrosion, A Wiley-Interscience Publication, 1973.
[38] I. Suzuki, N. Masuko, T. Hisamatsu, "Electrochemical properties of iron rust", Corros. Sci., vol. 19, 1979, pp. 521–535.
[39] Joseph T. Keiser, Chris W. Brown, "Charaterization of the passive film formed on weathering steels" C, Corros. Sci., vol. 23, 1983, pp. 251–259.
[40] I. Matsushima, T. Ueno, "On the protective nature of atmospheric rust on low alloy steel", Corros. Sci., vol. 11, 1971, pp. 129–140.

Ch. Thee was born in Nonthaburi, Thailand. He received M. Eng in Metallurgical Engineering from King Mongkut's University of Technology Thonburi, Thailand in 2005. He completed His D.Eng at Institute of Metal Research, University of Chinese Academy of Science (UCAS), China under the financial support from Thai Government. He is now a lecturer at the faculty of engineering, Burapha University, Chonburi, Thailand.